xCell: Digitally portraying the tissue cellular heterogeneity landscape

Dvir Aran, Zicheng Hu and Atul J. Butte

Institute for Computational Health Sciences, University of California, San Francisco, San Francisco, California, 94158, USA.

Contact information:

Dvir Aran: dvir.aran@ucsf.edu

Zicheng Hu: zicheng.hu@ucsf.edu

Atul J. Butte: atul.butte@ucsf.edu

The authors declare that there is no conflict of interest in relation to this article.

Abstract

Tissues are a complex milieu consisting of numerous cell types. For example, understanding the cellular heterogeneity the tumor microenvironment is an emerging field of research. Numerous methods have been published in recent years for the enumeration of cell subsets from tissue expression profiles. However, the available methods suffer from three major problems: inferring cell subset based on gene sets learned and verified from limited sources; displaying only partial portrayal of the full cellular heterogeneity; and insufficient validation in mixed tissues. To address these issues we developed *xCell*, a novel gene-signature based method for inferring 64 immune and stroma cell types. We first curated and harmonized 1,822 transcriptomic profiles of pure human cell types from various sources, employed a curve fitting approach for linear comparison of cell types, and introduced a novel spillover compensation technique for separating between closely related cell types. We test the ability of our model learned from pure cell types to infer enrichments of cell types in mixed tissues, using both comprehensive *in silico* analyses, and by comparison to cytometry immunophenotyping to show that our scores outperform previously published methods. Finally, we explore the cell type enrichments in tumor samples and show that the cellular heterogeneity of the tumor microenvironment uniquely characterizes different cancer types. We provide our method for inferring cell type abundances as a public resource to allow researchers to portray the cellular heterogeneity landscape of tissue expression profiles: http://xCell.ucsf.edu/.

Introduction

In addition to malignant proliferating cells, tumors are also composed of numerous distinct non-cancerous cell types and activation states of those cell types. This notion, which is termed the tumor microenvironment, has been in the spotlight of research in recent years and is being further explored by novel techniques. The most studied set of non-cancerous cell types are the tumor-infiltrating lymphocytes (TILs). However, these TILs are only part of a variety of innate and adaptive immune cells, stroma cells and many other cell types that are found in the tumor and interact with the malignant cells. This complex and dynamic microenvironment is now recognized to be important both in promoting and inhibiting of tumor growth, invasion, and metastasis [1,2]. Understanding the cellular heterogeneity composing the tumor microenvironment is key for improving existing treatments, the discovery of predictive biomarkers and development of novel therapeutic strategies.

Traditional approaches for dissecting the cellular heterogeneity in liquid tissues are difficult to apply in solid tumors [3]. Therefore, in the last decade, numerous methods have been published for digitally dissecting the tumor microenvironment using gene expression profiles [4–7] (Reviewed in [8]). Recently, multitudes of studies have been published applying published and novel techniques on publicly available resources of tumor samples such as The Cancer Genome Atlas (TCGA) [6,9–13]. There are two general types of techniques: deconvolving the complete cellular composition, and assessing enrichments of individual cell types.

There are at least seven major concerns that the *in silico* methods could be prone to errors, and cannot reliably portray the cellular heterogeneity of the tumor microenvironment. First, current techniques depend on the expression profiles of purified cell types to identify reference genes and therefore rely heavily on the data source of which the references are inferred from, and could be inclined to overfitting to these data. Second, current methods portray only a very narrow perspective of the tumor microenvironment. The available methods usually focus on a subset of immune cell types, thus not accounting for the further richness of cell types in the microenvironment, including blood vessels and other different forms of cell subsets [14,15]. A third problem is the ability of cancer cells to “imitate” other cell types by expressing immune-specific genes, such as macrophages-like expression pattern in tumors with parainflammation [16]; only a few of the methods take this into account. Fourth, the ability of existing methods to estimate cell abundance have not yet been comprehensively validated in mixed samples. Cytometry is a common method for counting cell types in a mixture, and when performed in combination with gene expression profiling, can allow validation of the estimations. However, in most studies that included cytometry validation, these analyses were performed on only a very limited number of cell types and a limited number of samples [7,13].

A fifth challenge is that deconvolution approaches are prone to many different biases because of the strict dependencies among all cell types that are inferred. This could highly affect reliability in analyzing tumor samples, which are prone to form non-conventional expression profiles. A sixth problem has been raised with inferring an increasing number of closely related cell types [10]. Finally, deconvolution analysis heavily relies on the structure of the reference matrix, which limits its application to the resource used to develop the matrix. One such deconvolution approach is CIBESORT, which is the most comprehensive study to date, allowing the enumeration of 22 immune subsets [7]. Newman et al. performed adequate evaluation across data sources and validated the estimations using cytometry immunophenotyping. However, the shortcomings of deconvolution approaches are apparent in CIBERSORT, which is limited to Affymetrix microarray studies.

On the other hand, gene set enrichment analysis is a simple technique, which can be easily applied across data types and can be quickly applied for cancer studies. Each gene signature is used independently from all other signatures; thus it is protected from the limitations of deconvolution approaches. However, because of this independence, it is many times hard to differentiate between closely related cell types. In addition, gene signature-based methods only provide enrichment scores, and thus do not allow comparison across cell types, and cannot allow insights on the abundance of the cell type in the mixture.

Here, we present *xCell*, a novel method that integrates the advantages of gene set enrichment with deconvolution approaches. We present a compendium of newly generated gene signatures for 64 cell types, spanning multiple adaptive and innate immunity cells, hematopoietic progenitors, epithelial cells and extracellular matrix cells derived from thousands of expression profiles. Using *in silico* mixtures, we transform the enrichment scores to a linear scale, and using a spillover compensation technique we reduce dependencies between closely related cell types. We evaluate these adjusted scores in RNA-seq and microarray data from primary cell types samples from various independent sources. We examine their ability to digitally dissect the tumor microenvironment by *in silico* analyses, and perform the most comprehensive comparison to date with cytometry immunophenotyping. We compare our inferences with available methods and show that scores from *xCell* are more reliable in digital dissection of mixed tissues. Finally, we apply our method on TCGA tumor samples to portray a full tumor microenvironment landscape across thousands of samples. We provide these estimations to the community and hope that this resource will allow researchers gain a better perspective of the complex cellular heterogeneity in tumor tissues.

Results

Generating a gene signature compendium of cell-types

To generate our compendium of gene signatures for cell types, we collected gene expression profiles from six sources: the FANTOM5 project, from which we annotated 719 samples from 39 cell types analyzed by the Cap Analysis Gene Expression (CAGE) technique [17]; the ENCODE project, from which we annotated 115 samples from 17 cell types analyzed by RNA-seq [18]; the Blueprint project, from which we annotated 144 samples from 28 cell types analyzed by RNA-seq (http://www.blueprint-epigenome.eu/); the IRIS project, from which we annotated 95 samples from 13 cell types analyzed by Affymetrix microarrays [19]; the Novershtern et al. study, from which we annotated 180 samples from 24 cell types analyzed by Affymetrix microarrays [20]; and the Human Primary Cells Atlas (HPCA), a collection of Affymetrix microarrays composed of many

Figure 1. xCell study design

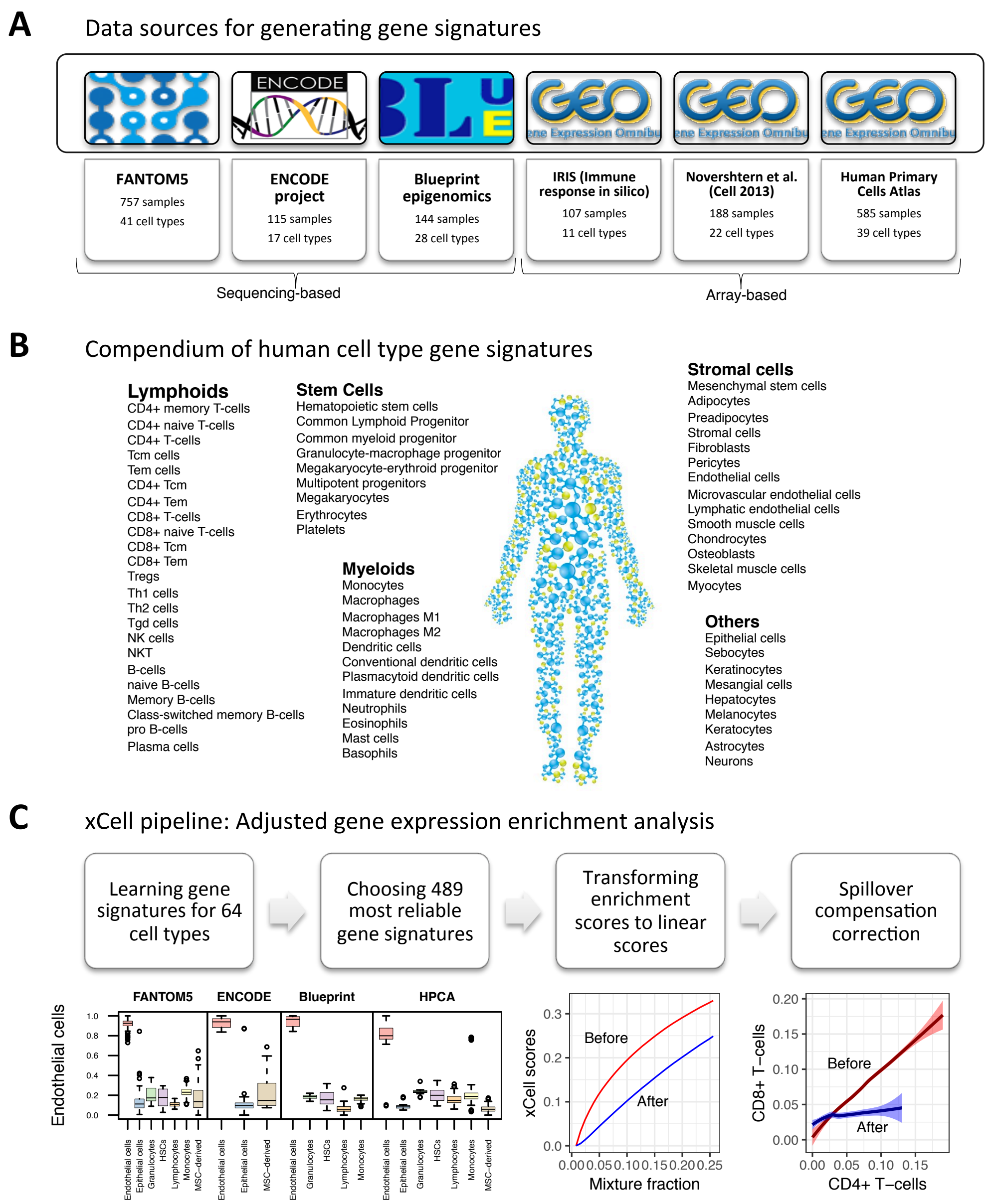

Figure 1. xCell study design. A. A summary of Data sources used in the study to generate the gene signatures, showing the number of pure cell types and number of samples curated from them. **B.** Our compendium of 64 human cell types gene signatures grouped into 5 cell types families. **C.** The xCell pipeline: Using the data source and based on different thresholds we learn gene signatures for 64 cell types. Of this collection of 5,327 signatures we choose 489 most reliable cell types, 3 for each cell types from each data source were it is available. The raw score is then the average ssGSEA score of all signatures corresponding to the cell type. Using simulations of gene expression for each cell type we learn a function to transform the non-linear association between the scores to a linear scale. Using the simulations we also learn the dependencies between cell types scores and apply a spillover compensation method to adjust the scores.

samples from 41 cell types [21] (Figure 1A). Altogether we collected and curated gene expression profiles from 1,822 samples of pure cell types, annotated to 64 distinct cell types and cell subsets (Figure 1B and Supplementary Table 1). Of those, 54 cell types were found in at least 2 of these data sources.

Our strategy for selecting reliable cell type gene signatures is shown in Figure 1C (see Methods for full description and technical details). For each data source independently we identified genes that are overexpressed in one cell type compared to all other cell types. We applied different thresholds for choosing set of genes to represent the cell type gene signatures; hence from each source, we generated dozens of signatures per cell type. This scheme yielded 5,327 gene signatures corresponding to 64 cell types. Importantly, since our primary aim is to develop a tool for studying the cellular heterogeneity in the tumor microenvironment, we applied a methodology we previously developed [16] to filter out genes that tend to be overexpressed in a set of 634 carcinoma cell lines from the Cancer Cell Line Encyclopedia (CCLE) [22].

Next, we used single-sample gene set enrichment analysis (ssGSEA) to score each sample based on all signatures. ssGSEA is a well-known method for aggregating a single score of the enrichment of a set of genes in the top of a ranked gene expression profile [23]. To choose the most reliable signatures we tested their performance in identifying the corresponding cell type in each of the data sources. To prevent overfitting, each signature learned from one data source was tested in other sources, but not in the data source it was originally inferred. To reduce biases resulting from a small number of genes and from the analysis of different platforms, instead of one signature per cell type, the top three ranked signatures from each data source were chosen. Altogether we generated 489 gene signatures corresponding to 64 cell types spanning multiple adaptive and innate immunity cells, hematopoietic progenitors, epithelial cells and extracellular matrix cells (Supplementary Table 2). The raw enrichment score per cell type is defined as the average ssGSEA scores from all the cell type's corresponding signature. Observing the scores in pure cell types affirmed their ability to identify the corresponding cell type compared to other cell types (Supplementary Figure 1).

Spillover compensation between closely related cell types

Our primary objective is to accurately identify enrichments of cell types in mixtures. To imitate such admixtures, we performed an array of simulations of gene expression combinations of cell types to assess the accuracy and sensitivity of our gene signatures. We generated such *in silico* expression profiles using different data sources, including data that was not part of the signatures generation; using different sets of cell types in mixtures; and by choosing randomly one sample per cell type from all available samples in the data source. The simulations revealed that our raw scores reliably predict even small changes in the proportions of cell types, easily distinguish between most cell types, and are reliable in different transcriptomic analysis platforms (Supplementary Figure 2). However, the simulations also revealed that raw scores of RNA-seq samples are not linearly associated with the abundance and that they do not allow comparisons across cell types (Supplementary Figure 3). Thus, using our simulations, we fit a formula that transforms the raw scores to cell-type abundances. We found that the transformed scores showed resemblance to the known fractions of the cell types in simulations, thus allowing to compare scores across cell types, and not just across samples (Supplementary Figure 4).

The simulations also revealed another limitation of the raw scores: closely related cell-types tend to have correlating scores (Supplementary Figure 4). That is, scores may show enrichment for a cell type due to a 'spillover effect' between closely related cell types. This problem mimics the spillover problem in flow-cytometry, in which fluorescent signals correlate with each other due to spectrum overlaps. Inspired by the compensations method used in flow-cytometry studies [24], we leveraged our simulations to generate a spillover matrix that allows correcting for correlations between cell types.

Figure 2. Evaluation of the performance of xCell using simulated mixtures

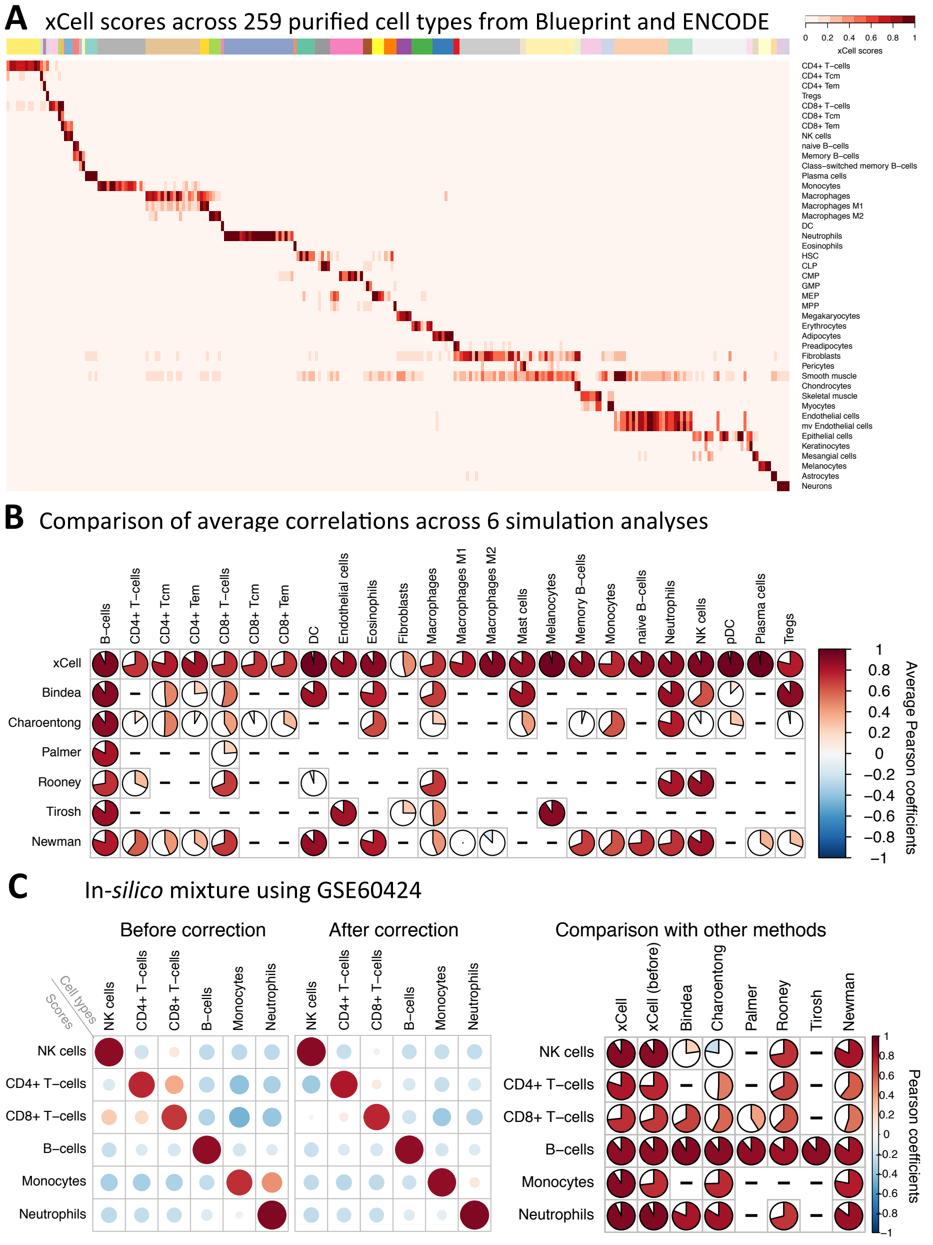

A xCell scores across 259 purified cell types from Blueprint and ENCODE

B Comparison of average correlations across 6 simulation analyses

C In-*silico* mixture using GSE60424

Figure 2. Evaluation of the performance of xCell using simulated mixtures. A. An overview of adjusted scores for of 43 cell type in 259 purified cell types samples from the Blueprint and ENCODE data sources (other data sources are in supplementary figure 4). Most signatures clearly distinguish the corresponding cell type from all other cell types. **B.** Average correlation coefficients of 24 cell types in 6 simulations using Blueprint, ENCODE and FANTOM5. Independent simulations are available in supplementary figure 4. The first row corresponds to our inferences in predicting the underlying abundances of the cell types in the simulations (both color and pie chart correspond to average Pearson coefficients). Bindea, Charoentong, Palmer, Rooney and Tirosh represent sets of signatures for cell types from the corresponding manuscripts. Newman is the inferences produced using CIBERSORT on the simulations. Here the averages do not include the FANTOM5 simulations, since CIBERSORT was not able to recover any signal. In all cell types, except regulatory T-cells, our inferences outperform all other methods. **C.** A simulation analysis using GSE60424 as the data source, which was not part of the development of xCell. This data source contains 114 RNA-seq samples from 6 major immune cell types. **Left:** Correlation coefficients using our method before spillover adjustment and after the adjustment. Dependencies between CD4+ T-cells, CD8+ T-cells and NK cells were greatly reduced; spillover from monocytes to neutrophils was also removed. **Right:** Same as B, but only based on the simulations using GSE60424. Our method outperforms all other methods in all 6 cell types.

To better compensate for low abundances in mixtures we created a simulated dataset where each sample contains 25% of the cell type of interest and the rest from a non-related cell type and produced a spillover matrix, a representation of the dependencies of scores between different cell types. Applying the spillover correction procedure on the pure cell types (Figure 2A and Supplementary Figure 1) and simulated expression profiles (Figure 2B-C and Supplementary Figure 4) showed that this method could successfully reduce associations between closely related cell types, and in general improved the associations between scores and abundance. This pipeline of generating adjusted cell type enrichment scores from gene expression profiles, which we named *xCell,* is available as an R package and a simple web tool: http://xCell.ucsf.edu/.

We next compared the *xCell* scores with a set of 53 previously published signatures corresponding to 26 cell types [6,12,25,26] (Supplementary Table 3). We applied each of the signatures in an array of simulations and compared their performance to estimate the simulated proportions (Supplementary Figure 4). Our analysis showed that *xCell* outperformed the previously published signatures in recapitulating the underlying abundances in 19 of the comparable cell types, only showing a slightly weaker ability to detect regulatory T-cells (Tregs) (Figure 2B and Supplementary Figure 4). It should be noted that the signature that performed better is based on one gene, FOXP3, and it is not clear if this gene can reliably predict the Tregs abundance in real mixtures, especially in samples where activated T cells are abundant [27]. These simulated mixtures were all performed using the data sources that were also used for generating our signatures; thus for the next step, we employed an independent data source of multiple cell types that was not part of the development of the method (GSE60424) [28]. Again, *xCell* inferences of the underlying abundances of the simulated mixtures outperformed all other signatures (Figure 2C). Importantly, our compensation technique was able to completely remove associations between cell types, while previously published signatures showed considerate dependencies between closely related cell types, such as between CD8+ T-cells and NK cells (Supplementary Figure 5).

In addition, we also compared *xCell* with CIBERSORT, a prominent deconvolution-based method [7]. Unlike signature-based methods, which output independent enrichment scores per cell type, the output from deconvolution-based methods is the inferred proportions of the cell types in the mixture. The L22 reference matrix of CIBERSORT was only calibrated to work with Affymetrix microarrays, nevertheless, it also performed well in our simulations generated using RNA-seq data from Blueprint, but not when using data from FANTOM5 (Supplementary Figure 4). Similar to the performance compared to signatures, *xCell* also outperformed CIBERSORT enumerations across all cell types, using both Blueprint and GSE60424 as data sources (Figure 2B-C and Supplementary Figure 4). *xCell* performed relatively well not just per cell types, but also in assessing proportions per sample, for example in a simulation using the Blueprint samples our scores showed a correlation of 0.67 on average across the 500 simulated mixtures compared to 0.44 using the CIBERSORT enumerations (Supplementary Figure 4).

Validation of enrichment scores with cytometry immunoprofilings

In addition to the simulated mixtures analysis, we compared our estimates for cell types enrichments from gene expression profiles with mass spectrometry (CyTOF) immunophenotyping. We utilized independent publicly-available studies, in which a total of 165 individuals were studied for both gene expression from whole blood and FACS across 18 cell subsets from peripheral blood mononuclear cells (PBMC) (available in ImmPort SDY311 and SDY420) [29]. We calculated *xCell* scores for each of the signatures using the study's expression profiles and correlated the scores with the FACS fractions of the cell subsets. Of the 14 cell types with at least 1% abundance, *xCell* was able to significantly recover 8 and 10 cell subsets in SDY311 and SDY420 respectively (Pearson correlation between calculated and actual cell counts *p-value* < 0.05) (Figure 3). Comparing the performance of *xCell* to previously published signatures and CIBERSORT revealed that no other method was able to recover cell types that our method was not able to recover in both data sets (Figure 3). In general, previous methods were able to recover signal only from major cell types, including B-cells, CD4+ and CD8+ T-cells, and monocytes, suggesting that their performance were not reliable in more specialized cell subsets. While our method also struggled in these cell subsets, it still showed significant correlations with most of the cell subsets, including effector memory CD8+ T-cells, naïve CD4+ T-cells and naïve B-cells. In addition, *xCell* was more reliable in CD4+ T-cells and monocytes and equally reliable in B-cells (Figure 3). In CD8+ T-cells *xCell* was outperformed by methods depending on solely on CD8A expression, which may not serve as a reliable biomarker in cancer settings (Supplementary Figure 6).

Figure 3. Comparison with flow-cytometry counts

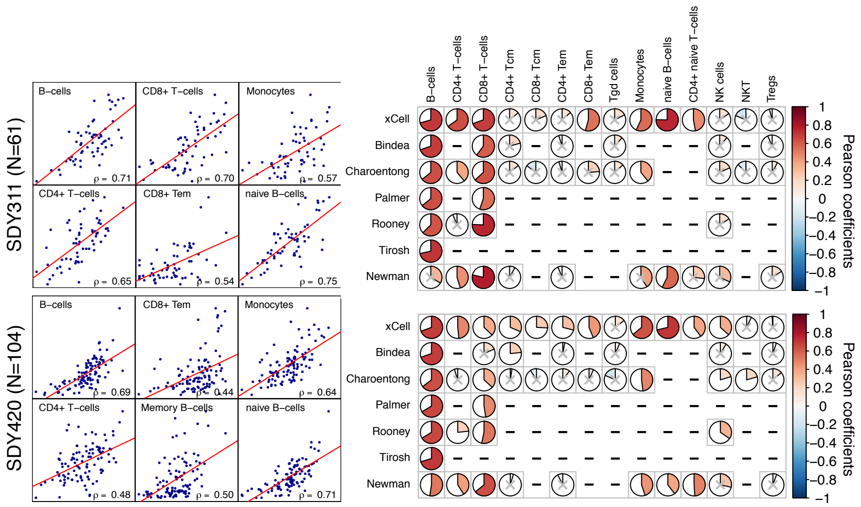

Figure 3. Compare digital dissection methods with flow cytometry counts. Right: Scatter plots of CyTOF fractions in PBMC vs. cell type scores from whole blood of 61 samples SDY311 (top) and 104 samples from SDY420 (bottom). Only top correlating cell types in each study is shown. **Right:** Correlation coefficients produced by our method compared to other methods. Only cell types with abundance of at least 1% on average, as measured by CyTOF, are shown. Non-significant correlations (p-value < 0.05) are marked with a gray 'x'.

Newman et al. [7] generated a smaller dataset of 20 samples analyzed by both gene expression and cytometry (available at GSE65133). *xCell* recovered 7 of the 8 measurements (*p-value* < 0.05) and was significantly more reliable in 4 of the cell types (Supplementary Figure 7).

Despite the generally improved abilities of *xCell* to estimate cell populations, we do note that in some cases the correlations we observed were relatively low, emphasizing the difficulty of estimating cell subsets in mixed samples, and the need for cautious examination and further validation of findings.

Cell types enrichments in tumor samples

We next applied our methodology on 8,875 TCGA primary tumor samples from twenty-four cancer types. We used the expression profiles devised by Rahman et al. [30], which include FPKM levels of twenty-two solid tumors and two liquid tumors (Supplementary Figure 8). Average scores of cell types in each cancer type affirmed our prior knowledge, validating the power of our method for identifying the cell type of origin of cancer types. As expected, epithelial cells were enriched in carcinomas, keratinocytes in squamous cell carcinomas, endothelial cells in clear cell carcinoma, hepatocytes in hepatocellular carcinoma, melanocytes in melanoma, B-cells in B-cells lymphoma, myeloid cells in AML and neurons in brain cancers (Figure 4A). While these results are expected, it is reassuring that *xCell* can be applied to and studied in human cancers.

Most of the cell types we infer are part of the complex cellular heterogeneity of the tumor microenvironment. We hypothesized that an additive combination of all cell types' scores would be negatively correlated with tumor purity. Thus, we generated a microenvironment score as the sum of all immune and stroma cell types. We then correlated this microenvironment score with our previously generated purity estimations, which are based on copy number variations, gene expression, DNA methylation and H&E slides [31]. Our analysis showed highly significant negative correlations in all cancer types, suggesting this score as a novel measurement for tumor microenvironment abundance (Supplementary Figure 9).

Figure 4. Cell types enrichments in cancer

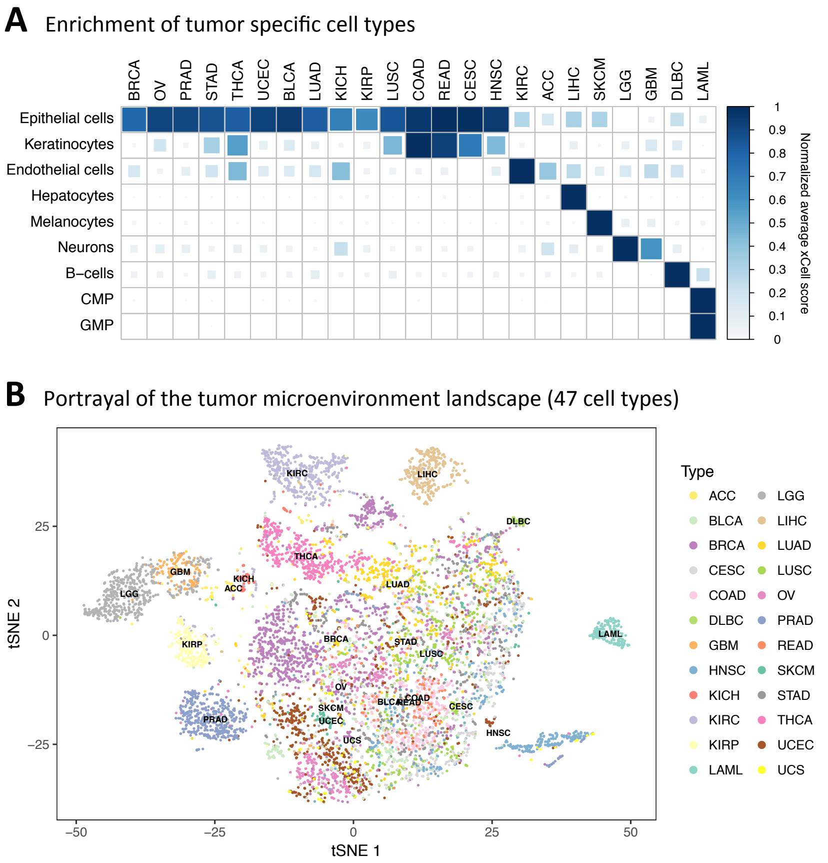

Figure 4. Cell types enrichment analysis in tumors. A. Average scores of 9 cell types across 24 cancer types from TCGA. Scores were normalized across rows. Signatures were chosen such that they are the cell of origin of cancer types or the most significant signature of the cancer type compared to all others. **B.** t-SNE plot of 8,875 primary cancer samples from TCGA colored by cancer type. The t-SNE plot was generated using the enrichment scores of 47 non-epithelial, non-stem cells and non-cell types specific scores. Many of the cancer type creates distinct cluster, emphasizing the important role of the tumor microenvironment in characterizing tumors

Finally, to provide insights into the potential of *xCell* to portray the tumor microenvironment, we plot all tumor samples based on their cell types scores. Using different sets of cell types inferences, we applied the t-Distributed Stochastic Neighbor Embedding (t-SNE) dimensionality reduction technique [32] (Supplementary Figure 10). Interestingly, the analysis revealed that unique microenvironment compositions characterize different cancer indications. For example, prostate cancer samples are easily distinguished based on their myeloid cell types composition, a unique lymphoid composition characterizes kidney cancers. Performing the analysis with all immune and stroma cell types revealed clear clusters distinguishing between most of the cancer types (Figure 4B), suggesting that the microenvironment composition uniquely characterizes cancer types. This notion emphasizes the importance of portraying the full cellular heterogeneity of the tumor microenvironment for the study of cancer. To this end, we calculated the enrichment scores for 64 cell types across the TCGA spectrum, and provide this data with the hope that it will serve the research community as a resource to further explore novel associations of cell types enrichment in human tumors (Supplementary Table 4).

Discussion

Recently, many studies have shown different methodologies for digital dissection of cancer samples [3,6,9–13]. These studies have suggested novel insights in cancer research and related to therapy efficacy. However, it is important to remember that the methods that have been applied for portraying the tumor microenvironment have only retained limited validation, and it is unclear how reliable their estimations are. In this study, we took a step back and focused on generating cell type gene scores that could reliably estimate enrichments of cell types. Our method, which is gene-signature based, is more reliable due to its reliance on a group of signatures for each cell type, learned from multiple data sources, which increases the ability to detect the signal from the noise. Our method also integrates a novel approach to remove dependencies between cell types, which allow better reliability in studying closely related cell types.

To develop *xCell*, we collected the most comprehensive resource to date of primary cell types, spanning the largest set of human cell types. We then performed an extensive validation of the predicted cell types inferences in mixed samples. Our method for choosing a set of signatures that are reliable across several data sources has proven to be beneficial, as our scores robustly outperformed all available methods in predicting the abundance of cell types in *in silico* mixtures and blood samples. Based on our evaluation, *xCell* provides the most accurate and sensitive way to identify enrichments of many cell types in an admixture, allowing the detection of subtle differences in the enrichments of a particular cell type in the tumor microenvironment with high confidence.

We chose to apply a gene signature enrichment approach over deconvolution methods because of several advantages that the former provides. First, gene signatures are rank-based, and therefore are suitable for cross-platform transcriptome measurements. We showed here that our scores reliably predict enrichments in different RNA-seq techniques and different microarrays platforms. They are agnostic to normalization methods or concerns related to batch effects, making them robust to both technical and biological noise. Second, there is no decline in performance with increasing number of cell types. The tumor microenvironment is a rich milieu of cell types, and our analyses show enrichments of many mesenchymal derived cells in the tumors. A partial portrayal of the tumor microenvironment may result in misleading findings. Finally, gene signatures are simple and can easily be adjusted.

The main disadvantage of gene signatures is their difficulty to discriminate closely related cell types, though it is not clear how well other methods can distinguish such cell types as well [10]. Our method takes this into account and uses a novel technique, inspired by flow cytometry analyses, to remove such dependencies between closely related cell types. It is important to note that until this step the cell types scores are independent of each other, and a deflection of genes of one cell type will not harm all other cell types. However, the 'spillover correction' adjustment removes this strict independence between cell types inferences as in deconvolution methods. While our method only compensates between closely related cell types and is, therefore, most of the inferences are still independent, the results should yet be cautiously analyzed.

Despite the utility of our signatures for characterizing the tumor microenvironment, several issues require further investigation. While our signatures outperformed previous methods, it is important to note that our correlations were still far from perfect with direct measurements. More expression data from pure cell types, especially cell types with limited samples, and more expression data coupled with cytometry counts from various tissue types will allow defining signatures more precisely and in turn, allow better reliability. Meanwhile, it is necessary to refer to inferences made by our method or other methods with a grain of salt. Discoveries made using digital dissection methods must be rigorously validated using other technologies to avoid hasty conclusions.

In summary, tissue dissection methods are an emerging tool for large-scale characterization of the tumor cellular heterogeneity. These approaches do not rely on tissue dissociation, opposed to single-cell techniques, and therefore provide an effective tool for dissecting solid tumors. The immense availability of public gene expression profiles allows these methods to be efficiently performed on hundreds of historical cohorts spanning thousands of patients, and to associate them with clinical outcomes. Here we presented the most comprehensive collection of gene expression enrichment scores for cell types. Our methodology for generating cell type enrichment scores and adjusting them to cell types proportions allowed us to create a powerful tool that is the most reliable and robust tool currently available for identifying cell types across data sources. We provide a simple web tool to the community and hope that further studies will utilize it for the discovery of novel predictive and prognostic biomarkers, and new therapeutic targets: http://xCell.ucsf.edu/.

Methods

Data sources

Signatures data sources: RNA-seq and cap analysis gene expression (CAGE) normalized FPKM were downloaded from the FANTOM5, ENCODE and Blueprint data portals. Raw Affymetrix microarray CEL files were downloaded from the Gene Expression Omnibus (GEO), accessions: GSE22886 (IRIS), GSE24759 (Novershtern) and GSE49910 (HPCA), and analyzed using the Robust Multi-array Average (RMA) procedure on probe-level data using Matlab functions. The analysis was performed using custom CDF files downloaded from Brainarray [33]. All samples were manually annotated to 64 cell types (Supplementary Table 1).

Other expression data sources: RNA-seq normalized counts were downloaded from the gene expression omnibus (GEO) accession GSE60424. Illumina HumanHT-12 V4.0 beadchip data of PBMC samples and the accompanying CyTOF data were downloaded from ImmPort accession SDY311, and quantile normalized using Matlab functions. Similarly, Agilent Whole Human Genome 4 x 44 K slides data of PBMC samples and the accompanying CyTOF data were downloaded from ImmPort accession SDY420 [34], and quantile normalized using Matlab functions. Multiple probes per gene were collapsed using averages. RNA-seq data of Cancer Cell Line Encyclopedia (CCLE) [22] was obtained using the PharmacoGx R package [35]. FPKM levels of 9,264 TCGA samples were downloaded from GEO accession GSE62944, and non-primary tumor samples were removed.

Published signatures were collected from their corresponding papers [6,12,25,26]. (Supplementary Table 3).

In silico mixtures

The simulations were performed as following: A mixture set contains 500 mixtures (simulated expression profiles) that were generated using one of the data sources. First, we choose a representative group of cell types available in the data. Second, in each of the mixtures we randomly chose one sample for each cell type to represent the expression profile of the cell type. This random selection introduces significant noise to the mixture, and between mixtures in the mixture set, which reflect the variation we observe between real datasets. We then randomly choose a fraction for each of the cell types (the fractions sum to 1). The expression profile of each cell type is multiplied by its corresponding fraction, and the expression profile of the mixture is the sum of all cell types. This process is repeated 500 times to create 500 distinct mixtures using same set of cell types. We also created simulated mixtures that use the median expression profile of a cell type instead of choosing randomly one of the samples. This creates significantly homogenous and noiseless mixture, and the signatures can precisely identify small differences.

The xCell pipeline

Filtering cancer genes: In a previous study [16] we calculated using CCLE the number of cell lines that are over-expressing each gene (2-fold more than the peak of expression distribution). For generating the signatures we only use genes that have an overexpression rate of less than 5% (less than 32 cell lines of the 634 carcinoma cell lines). We use this stringent threshold to eliminate genes that tend to be overexpressed in tumors, regardless of the cellular composition. Of 18,988 genes analyzed, 9,506 genes were identified as not overexpressing in tumors. For signatures of cell types that may be the cell of origin of solid tumors, including epithelial cells, sebocytes, keratinocytes, mesangial cells, hepatocytes, melanocytes, astrocytes and neurons we used all genes.

Generating gene signatures: Expression profiles were reduced to 10,782 genes that are shared across all 6 data sources. Gene expression was converted to log scale by adding 3 and then $\log_2$ conversion. In each group of samples corresponding to a cell type we calculated 10th, 25th, 33.3th, 50th percentiles of low expression ($Q1_q$), and 90th,75th, 66.6th, 50th quantiles of high expression ($Q2_{1-q}$),q=10%,25%,33.3%,50%.=. For cell type *A* we calculated the difference for each gene between $Q1_q$(A) and max($Q2_{1-q}$(all other cell types)). We repeated this also for second and third largest $Q2_{1-q}$(all other cell types). The signature of cell type *A* consists of all genes that pass a threshold. We used different thresholds here: 0, 0.1, log2(1.5), log(2), log2(3), log2(4). We repeated this procedure to each of the 6 data sources independently. Only gene sets of at least 10 genes and no more than 200 genes were reserved. This scheme yielded 5,327 gene signatures corresponding to 64 cell types. We calculated single-sample gene set enrichment analysis (ssGSEA) for each of those signatures to score each sample in each of the data sources using the GSVA R package [36].

Choosing the "best" signature: For each signature we computed the t-statistic between the scores of the corresponding cell type compared to all other samples, omitting samples from parental or descendant cell types (for CD4+ naïve T-cells the general CD4+ T-cells are not used in the calculations). The procedure was performed in each data source where the corresponding cell type was available, except the data source from which the signature was learned. Thus, a signature is only chosen if it is reliable in a data source were it was not trained upon. If the cell type is available in only one data source, the signature was tested in that data source. From each data source the top 3 signatures were chosen. All together we chose 489 signatures corresponding to 64 cell types (across the 6 data sources we have 163 cell types) (Supplementary Table 2). The raw score for a cell type is the average of all corresponding signatures.

Learning parameters for raw scores transformation: For each cell type we created a synthetic mixture using the median expression profile of the cell type (cell *X*) and an additional 'control' cell type. For 'control' we used multipotent progenitor (MPP) cell samples or endothelial cell samples, because both are found in all the sequencing-based data sets. We generated such mixtures using increasing levels of the corresponding cell type (0.8% of the cell *X* and 99.2% control, 1.6% cell *X* and 98.4% control, etc.). We noticed two problems with the raw scores: ssGSEA scores have different distributions between different signatures, thus a score from a signatures cannot be compared with a score from another signature. In addition, in RNA-seq data, the association between the underlying levels of the cell type was not linearly associated with the score. We thus designed a transformation pipeline for the scores – for each cell type, using the synthetic mixtures we first shifted the scores to 0 using the minimal score (which corresponded to mixtures containing 0.8% of the cell type) and divided by 5000. We then fit a power function to the scores ranging corresponding to abundances of 0.8% to 25.6%. We used this range because we are mostly interested in identifying cell types with low abundance, and above that the function exponential increase may interfere in a precise fitting. The power coefficient is then averaged across the data sources were the cell type is available.

Learning the spillover compensation reference matrix: Another limitation that was observed in the mixtures is the dependencies between closely related cell types: scores that predict enrichment of one cell type also predict enrichment of another cell type, which might not even be in the mixture. To overcome this problem we created a reference matrix of 'spillovers' between cell types. We creating a synthetic mixture set, where each mixture that contains 25% of each of the cell types (median expression) and 75% of a 'control' cell type. We calculated raw cell types scores and transformed them using the learned coefficients as explained above (P – power coefficients vector). We combined all sequencing-based data sources together by using the average scores, and added samples from cell types that are not in any of the sequencing-based data sources as well to have a full matrix of 64x64, where rows are cell types scores and column are cell type samples (K – spillover matrix). We then normalize each row of cell types scores by the score of corresponding cell type. In another words, we normalized the matrix by the diagonal. This diagonal vector is then used as calibration vector in generating the final scores (V - calibration vector). The 'spillover' between a cell type score (*x*) and another cell types (*y*) is the ratio between *x* and *y*. We only take into account spillover between cell types from the same family (immune, hematopoietic stem cells and non-immune); parent cell types are only compensated between other parent cell types (CD4+ T-cells are compensated against CD8+ T-cells, but not CD8+ Tem); child cell types are only compensated compared to other child cell types from the same parent. The spillover matrix, power and calibration coefficients are available in Supplementary Table 5.

Calculating scores for a mixture:

Input: Gene expression data set, rows are genes and columns are samples (N – number of samples). Duplicate gene names are combined together. (1) Calculating ssGSEA for each of the 489 gene signatures. (2) Averaging scores of all signatures corresponding to a cell type. The result is a matrix (*A*) with 64 rows and N columns. (3) Each element in the scores matrix (A_{ij}) is transformed using the following formula:

$$T_{ij} = \left(A_{ij} - \min(A_i)\right)/(5000 * V_i)^{P_i}$$

The output is matrix *T* of transformed scores. If the input is microarray based, P is not used. (4) Spillover compensation is then performed for each row using linear least squares that minimizes the following:

$$\|K \cdot x - T_i\|, \text{ such that } x \geq 0$$

All *x*'s are then combined to create the final xCell scores.

Cytometry analyses

Gene expression and cytometry data were downloaded from ImmPort (SDY311 and SDY420). The gene expression data was quantile normalized using Matlab functions, and multiple probes per gene were collapsed using averages. The cytometry data counts were divided by the viable/singlets counts. In the SDY311 dataset 10 patients had two replicates of expression profiles, and those were averaged. Two outlier samples in the cytometry data set were removed from further analyses (SUB134240, SUB134283).

Other tools

The CIBERSORT web tool was used for inferring proportions using the expression profile (http://cibersort.stanford.edu). CIBERSORT results of activated and resting cell types were combined, B-cell and CD4+ T-cells percentages are the combination of all their subtypes. t-SNE plots were produced using the Rtsne R package. Purity measurements were obtained from our previous publication [31]. Correlation plots were generated using the corrplot R package.

Supplementary Information

Supplementary Figure 1. Reliability of cell types signatures across data sources before and after adjustments. Boxplots of the ssGSEA scores of each of the 64 cell types scores across the 6 data sources. Red boxplots represent the corresponding cell type; blue boxplots represent parental or descendant cell types. Each page presents the raw scores in each pure cell type (top) and the adjusted scores (bottom).

Supplementary Figure 2. Simulated mixtures of pure cell types inferred by raw xCell scores. Scatter plots of inferred vs. simulated abundance in 10 mixtures sets.

Supplementary Figure 3. Transformation procedure of raw scores to linear scales. The associations between raw scores and simulated abundances before and after transformation.

Supplementary Figure 4. Cell types inferences in gene expression simulations. Simulations analyses, showing the correlation between cell types based on our inferences compared to other methods.

Supplementary Figure 5. Dependencies between CD8+ T-cells and NK cells. An example of dependency between cell types in published signatures.

Supplementary Figure 6. CD8+ T-cells scores vs. CD8A expression in cancer cell lines. An example of the problem of using a single gene for predicting cell type abundance.

Supplementary Figure 7. Comparison of xCell, CIBERSORT and flow cytometry counts in GSE65133. Additional cytometry and expression data set used in the CIBERSORT study.

Supplementary Table 1. Summary table of primary cell types used in this study. Number of samples annotated for each of the 64 cell types across the 6 data sources.

Supplementary Table 2. 489 cell type gene signatures.

Supplementary Table 3. 53 previously published cell type gene signatures.

Supplementary Table 4. xCell scores in 9,264 samples from TCGA.

Supplementary Table 5. Spillover matrix and calibrating coefficients.

Competing interests

The authors declare no competing financial interests.

Acknowledgments

We thank Marina Sirota and Thomas Peterson for helpful discussions. This work was supported by the Gruss Lipper Postdoctoral Fellowship to D.A., and the National Cancer Institute (U24 CA195858) and the National Institute of Allergy and Infectious Diseases (Bioinformatics Support Contract HHSN272201200028C) to A.J.B. The content is solely the responsibility of the authors and does not necessarily represent the official views of the National Institutes of Health.

References

1. Galon J, Costes A, Sanchez-Cabo F, Kirilovsky A, Mlecnik B, Lagorce-Pagès C, et al. Type, density, and location of immune cells within human colorectal tumors predict clinical outcome. Sci. (New York, NY) [Internet]. 2006;313:1960–4. Available from: papers3://publication/doi/10.1126/science.1129139

2. Hanahan D, Coussens LM. Accessories to the Crime: Functions of Cells Recruited to the Tumor Microenvironment. Cancer Cell. 2012. p. 309–22.

3. Gentles AJ, Newman AM, Liu CL, Bratman S V, Feng W, Kim D, et al. The prognostic landscape of genes and infiltrating immune cells across human cancers. Nat. Med. [Internet]. 2015;21:938–45. Available from: http://www.ncbi.nlm.nih.gov/pubmed/26193342

4. Abbas AR, Wolslegel K, Seshasayee D, Modrusan Z, Clark HF. Deconvolution of blood microarray data identifies cellular activation patterns in systemic lupus erythematosus. PLoS One. 2009;4.

5. Shen-Orr SS, Gaujoux R. Computational deconvolution: extracting cell type-specific information from heterogeneous samples. Curr. Opin. Immunol. [Internet]. 2013 [cited 2015 Mar 24];25:571–8. Available from: http://www.sciencedirect.com/science/article/pii/S0952791513001507

6. Rooney MS, Shukla SA, Wu CJ, Getz G, Hacohen N. Molecular and genetic properties of tumors associated with local immune cytolytic activity. Cell. 2015;160:48–61.

7. Newman AM, Liu CL, Green MR, Gentles AJ, Feng W, Xu Y, et al. Robust enumeration of cell subsets from tissue expression profiles. Nat. Methods [Internet]. 2015 [cited 2015 Mar 30];12:453–7. Available from: http://www.ncbi.nlm.nih.gov/pubmed/25822800

8. Newman AM, Alizadeh AA. High-throughput genomic profiling of tumor-infiltrating leukocytes. Curr. Opin. Immunol. 2016;41:77–84.

9. Angelova M, Charoentong P, Hackl H, Fischer ML, Snajder R, Krogsdam AM, et al. Characterization of the immunophenotypes and antigenomes of colorectal cancers reveals distinct tumor escape mechanisms and novel targets for immunotherapy. Genome Biol. [Internet]. 2015;16:64. Available from: http://genomebiology.com/2015/16/1/64

10. Li B, Severson E, Pignon J-C, Zhao H, Li T, Novak J, et al. Comprehensive analyses of tumor immunity: implications for cancer immunotherapy. Genome Biol. 2016;17:14.

11. Iglesia MD, Parker JS, Hoadley KA, Serody JS, Perou CM, Vincent BG. Genomic Analysis of Immune Cell Infiltrates Across 11 Tumor Types. J. Natl. Cancer Inst. [Internet]. Oxford University Press; 2016 [cited 2016 Aug 10];108:djw144. Available from: http://jnci.oxfordjournals.org/lookup/doi/10.1093/jnci/djw144

12. Charoentong P, Finotello F, Angelova M, Mayer C, Efremova M, Rieder D, et al.

Pan-cancer Immunogenomic Analyses Reveal Genotype-Immunophenotype Relationships and Predictors of Response to Checkpoint Blockade. Cell Rep. 2017;18:248–62.

13. Şenbabaoğlu Y, Gejman RS, Winer AG, Liu M, Van Allen EM, de Velasco G, et al. Tumor immune microenvironment characterization in clear cell renal cell carcinoma identifies prognostic and immunotherapeutically relevant messenger RNA signatures. Genome Biol. [Internet]. 2016 [cited 2017 Feb 1];17:231. Available from: http://genomebiology.biomedcentral.com/articles/10.1186/s13059-016-1092-z

14. Pattabiraman DR, Weinberg RA. Tackling the cancer stem cells - what challenges do they pose? Nat. Rev. Drug Discov. [Internet]. 2014;13:497–512. Available from: http://www.ncbi.nlm.nih.gov/pubmed/24981363%5Cnhttp://dx.doi.org/10.1038/nrd4253

15. Turley SJ, Cremasco V, Astarita JL. Immunological hallmarks of stromal cells in the tumour microenvironment. Nat. Rev. Immunol. [Internet]. 2015;15:669–82. Available from: http://www.ncbi.nlm.nih.gov/pubmed/26471778

16. Aran D, Lasry A, Zinger A, Biton M, Pikarsky E, Hellman A, et al. Widespread parainflammation in human cancer. Genome Biol. [Internet]. BioMed Central; 2016 [cited 2016 Jul 21];17:145. Available from: http://genomebiology.biomedcentral.com/articles/10.1186/s13059-016-0995-z

17. Lizio M, Harshbarger J, Shimoji H, Severin J, Kasukawa T, Sahin S, et al. Gateways to the FANTOM5 promoter level mammalian expression atlas. Genome Biol. [Internet]. 2015;16:22. Available from: http://genomebiology.com/2015/16/1/22

18. Consortium EP, Bernstein BE, Birney E, Dunham I, Green ED, Gunter C, et al. An integrated encyclopedia of DNA elements in the human genome. Nature [Internet]. 2012;489:57–74. Available from: http://www.nature.com/doifinder/10.1038/nature11247%5Cnpapers3://publication/doi/10.1038/nature11247

19. Abbas AR, Baldwin D, Ma Y, Ouyang W, Gurney A, Martin F, et al. Immune response in silico (IRIS): immune-specific genes identified from a compendium of microarray expression data. Genes Immun. [Internet]. 2005;6:319–31. Available from: http://www.ncbi.nlm.nih.gov/pubmed/15789058

20. Novershtern N, Subramanian A, Lawton LN, Mak RH, Haining WN, McConkey ME, et al. Densely interconnected transcriptional circuits control cell states in human hematopoiesis. Cell. 2011;144:296–309.

21. Mabbott NA, Baillie JK, Brown H, Freeman TC, Hume DA. An expression atlas of human primary cells: inference of gene function from coexpression networks. BMC Genomics [Internet]. 2013;14:632. Available from: http://www.pubmedcentral.nih.gov/articlerender.fcgi?artid=3849585&tool=pmcentrez&rendertype=abstract

22. Barretina J, Caponigro G, Stransky N, Venkatesan K, Margolin AA, Kim S, et al. The Cancer Cell Line Encyclopedia enables predictive modelling of anticancer drug sensitivity. Nature [Internet]. 2012;483:603–7. Available from: http://dx.doi.org/10.1038/nature11003

23. Barbie DA, Tamayo P, Boehm JS, Kim SY, Moody SE, Dunn IF, et al. Systematic RNA interference reveals that oncogenic KRAS-driven cancers require TBK1. Nature [Internet]. 2009;462:108–12. Available from: http://www.pubmedcentral.nih.gov/articlerender.fcgi?artid=2783335&tool=pmcentrez&rendertype=abstract

24. Bagwell CB, Adams EG. Fluorescence spectral overlap compensation for any number of flow cytometry parameters. Ann. N. Y. Acad. Sci. [Internet]. 1993 [cited 2017 Feb 5];677:167–84. Available from: http://www.ncbi.nlm.nih.gov/pubmed/8494206

25. Bindea G, Mlecnik B, Tosolini M, Kirilovsky A, Waldner M, Obenauf AC, et al. Spatiotemporal dynamics of intratumoral immune cells reveal the immune landscape in human cancer. Immunity. 2013;39:782–95.

26. Tirosh I, Izar B, Prakadan SM, Wadsworth MH, Treacy D, Trombetta JJ, et al. Dissecting the multicellular ecosystem of metastatic melanoma by single-cell RNA-seq. Science (80-.). [Internet]. 2016;352:189–96. Available from: http://science.sciencemag.org.gate2.inist.fr/content/352/6282/189.abstract

27. Ziegler SF. FOXP3: Not just for regulatory T cells anymore. Eur. J. Immunol. [Internet]. 2007 [cited 2017 Feb 4];37:21–3. Available from: http://www.ncbi.nlm.nih.gov/pubmed/17183612

28. Linsley PS, Speake C, Whalen E, Chaussabel D. Copy Number Loss of the Interferon Gene Cluster in Melanomas Is Linked to Reduced T Cell Infiltrate and Poor Patient Prognosis. Castro MG, editor. PLoS One [Internet]. 2014 [cited 2017 Feb 2];9:e109760. Available from: http://www.ncbi.nlm.nih.gov/pubmed/25314013

29. Bhattacharya S, Andorf S, Gomes L, Dunn P, Schaefer H, Pontius J, et al. ImmPort: Disseminating data to the public for the future of immunology. Immunol. Res. 2014;58:234–9.

30. Rahman M, Jackson LK, Johnson WE, Li DY, Bild AH, Piccolo SR. Alternative preprocessing of RNA-Sequencing data in the Cancer Genome Atlas leads to improved analysis results. Bioinformatics. 2015;31:3666–72.

31. Aran D, Sirota M, Butte AJ. Systematic pan-cancer analysis of tumour purity. Nat. Commun. [Internet]. 2015;6:8971. Available from: http://www.nature.com/doifinder/10.1038/ncomms9971

32. van der Maaten L, Hinton GE. Visualizing high-dimensional data using t-SNE. J. Mach. Learn. Res. [Internet]. 2008;9:2579–605. Available from: http://www.ncbi.nlm.nih.gov/entrez/query.fcgi?db=pubmed&cmd=Retrieve&dopt=AbstractPlus&list_uids=7911431479148734548related:VOiAgwMNy20J

33. Dai M, Wang P, Boyd AD, Kostov G, Athey B, Jones EG, et al. Evolving gene/transcript definitions significantly alter the interpretation of GeneChip data. Nucleic Acids Res. 2005;33.

34. Whiting CC, Siebert J, Newman AM, Du H, Alizadeh AA, Goronzy J, et al. Large-Scale and Comprehensive Immune Profiling and Functional Analysis of Normal Human Aging. Unutmaz D, editor. PLoS One [Internet]. 2015 [cited 2017 Feb 6];10:e0133627. Available from: http://www.ncbi.nlm.nih.gov/pubmed/26197454

35. Smirnov P, Safikhani Z, El-Hachem N, Wang D, She A, Olsen C, et al. PharmacoGx: an R package for analysis of large pharmacogenomic datasets. Bioinformatics [Internet]. 2016 [cited 2017 Feb 6];32:1244–6. Available from: http://www.ncbi.nlm.nih.gov/pubmed/26656004

36. Hänzelmann S, Castelo R, Guinney J. GSVA: gene set variation analysis for microarray and RNA-seq data. BMC Bioinformatics [Internet]. 2013;14:7. Available from: http://www.pubmedcentral.nih.gov/articlerender.fcgi?artid=3618321&tool=pmcentrez&rendertype=abstract